Title
High-Resolution in the Soft X-Ray Range from a Toroidal Grating Monochromator

Journal
Review of Scientific Instruments, 64(9)

Authors
Reich, Tobias
Hussain, Z.
Moler, E.J.
et al.

Publication Date
1993-03-01

LBL-33629
UC-401
Preprint

Lawrence Berkeley Laboratory
UNIVERSITY OF CALIFORNIA

CHEMICAL SCIENCES DIVISION

Submitted to Review of Scientific Instruments

High Resolution in the Soft X-Ray Range from a Toroidal Grating Monochromator

T. Reich, Z. Hussain, E. Moler, M. Blackwell, G. Kaindl,
D.A. Shirley, and M.R. Howells

March 1993

Prepared for the U.S. Department of Energy under Contract Number DE-AC03-76SF00098

DISCLAIMER

LBL-33629
UC-401

HIGH RESOLUTION IN THE SOFT X-RAY RANGE FROM A TOROIDAL GRATING MONOCHROMATOR

T. REICH[#,§], Z. HUSSAIN[#], E. MOLER[#], M. BLACKWELL[#], G. KAINDL[#,¥], D. A. SHIRLEY[§], AND M. R. HOWELLS[¶]

[#]CHEMICAL SCIENCES DIVISION
and
[¶]ACCELERATOR & FUSION RESEARCH DIVISION
Lawrence Berkeley Laboratory
University of California
Berkeley, California 94720

[§]DEPARTMENT OF CHEMISTRY AND PHYSICS
Pennsylvania State University
University Park, Pennsylvania 16802

[¥]INSTITUT FÜR EXPERIMENTALPHYSIK
Freie Universität Berlin
D-1000 Berlin 33

MARCH 1993

This work was supported by the Director, Office of Energy Research, Office of Basic Energy Sciences, Chemical Sciences Division, of the U.S. Department of Energy, LBL under Contract No. DE-AC03-76SF00098.

ABSTRACT

A resolving power, $E/\Delta E$, of $\geq$ 13,000 has been achieved with the modified 6m/160° Toroidal Grating Monochromator (TGM) installed on Beam Line 8-1 at the Stanford Synchrotron Radiation Laboratory (SSRL). The resolving power of the TGM was increased by replacing the entrance and exit slits with high-precision slits, masking the horizontal part (short radius) of the grating, and improving the TGM scanning mechanisms. To determine the performance of the monochromator, we measured the dependences of resolution and photon flux on the entrance and exit slit widths, the exit slit position, and the masking of the grating. The monochromator resolution in the energy range of 25 - 65 eV was derived from photoionization measurements of extremely narrow core-excitation resonances in He and Ne. With 10 micron vertical entrance and exit slit widths and 32 % mask opening of the grating, the monochromator has a resolution (FWHM) of 5.0±0.7 meV at a photon energy of 64.5 eV and a flux of 2×10^7 photons/sec/100 mA. The results suggest a simple procedure for converting a TGM with moderate resolution into a high-resolution monochromator with a moderate reduction in photon flux due to masking the grating, beyond the reduction attributable to the slit widths.

1. Introduction

Toroidal Grating Monochromators (TGM's) have been extensively used in various synchrotron radiation facilities. The TGM is generally known to have a moderate energy resolution with a high throughput [1-5]. In the standard configuration for a TGM [3, 4], mirrors focus the source sagitally and tangentially onto the entrance slit of the monochromator. The beam is then dispersed and focused onto the exit slit by the grating and refocused onto the sample by a bent cylindrical mirror. Various parameters of the instrument are optimized to sustain both very good resolution at the two wavelengths of the perfect focus and a moderate resolution over the entire energy range. As an improvement to this design, a movable exit slit can be adjusted to eliminate the vertical defocus for all wavelengths [6]. The contribution of aberrations to the resolution can be reduced further by masking a part of the toroidal grating. This will convert the TGM into a high-resolution monochromator at the cost of some photon intensity.

In Section 2, we give a brief theoretical analysis of the main terms which determine the resolution of the TGM. The monochromator design and necessary improvements to achieve high resolution are discussed in Section 3. The experimental techniques for measuring the resolution and the photon flux are given in Section 4. The performance of the monochromator is reported in Section 5. Section 6 gives the conclusions.

2. TGM Analysis

The parameters which determine the resolution can be understood from the analysis of the aberration-corrected, holographically produced toroidal grating. Following Noda et al. [7], we define the coordinate system as given in Fig. 1. The optical path function, F, for the ray from the source point, $A(x,y,z)$, through the point at the grating surface, $P(\xi,w,l)$, to the image point, $B\ (x',y',z')$, can be expressed as a power series in the aperture coordinates w,l [7]:

$$F = wF_{100} + lF_{011} + \tfrac{1}{2}w^2F_{200} + \tfrac{1}{2}l^2F_{020} + \tfrac{1}{2}w^3F_{300}$$
$$+\tfrac{1}{2}wl^2F_{120} + wlF_{111} + \tfrac{1}{8}w^4F_{400} + \tfrac{1}{4}w^2l^2F_{220} \qquad (1)$$
$$+\tfrac{1}{8}l^4F_{040} + \tfrac{1}{4}w^2F_{202} + \tfrac{1}{4}l^2F_{022} + \tfrac{1}{2}l^3F_{031} + \tfrac{1}{2}w^2lF_{211} + \ldots,$$

where i, j, and k in F_{ijk} are the powers of w, l, and z(or z') in the series expansion of F. Each F_{ijk} corresponds to some particular type of aberration and are exactly those given in Ref. [7]. The terms which have $j+k=odd$ have been omitted, being equal to zero by symmetry. Terms with $i=j=0$ are omitted because they do not represent aberrations. If we consider only the point A in the x, y plane ($z=0$) and assume that the astigmatism is reasonably well corrected ($z'\approx 0$), we can simplify Eq. (1). For the special case $z=z'=0$, the optical path function F can be written as

$$F' = \sum_{ij} F'_{ij} w^i l^j = w^2F'_{20} + l^2F'_{02} + wl^2F'_{12} + \text{higer order terms.} \qquad (2)$$

The power series terms, F'_{ij}, can be separated into a holographic contribution, H_{ij}, and a term, M_{ij}, due to a classically ruled grating [7]:

$$F'_{ij} = M_{ij} + \frac{m\lambda}{\lambda_0} H_{ij}, \qquad (3)$$

where m is the spectral order and λ_0 is the wavelength of the laser light used in constructing the holographic grating. The expressions for M_{ij} and H_{ij} which are relevant in our discussion are given in Table 1. Assuming a_{02} ($a_{20}=1/(2\rho)$) is chosen to correct the astigmatism (F'_{02}) for the entire wavelength region, the most important resolution-limiting aberrations are the defocus ($F'_{20}w^2$) and astigmatic coma ($F'_{12}wl^2$) which can be minimized by reducing the ruled width ($2w$) and the groove length ($2l$), respectively. The expression for the focusing term F'_{20}

$$F'_{20} = \left[\left(\frac{1}{2}\frac{\cos^2\alpha}{r} - a_{20}\cos\alpha\right) + \left(\frac{1}{2}\frac{\cos^2\beta}{r'} - a_{20}\cos\beta\right)\right] + \frac{m\lambda}{\lambda_0} H_{20} \qquad (4)$$

shows that for a given wavelength (α and β) and entrance arm length, r, the exit-slit distance ,r', can be determined so that F'_{20} is equal to zero.

This condition for a focus in the vertical plane of dispersion can be achieved over the whole wavelength region with a movable exit slit.

By differentiating the grating equation with respect to β at constant α, we can derive an expression for the slit-width limited monochromator resolution:

$$\Delta\lambda = \frac{\cos\beta}{Nmr'}\Delta Y, \qquad (5)$$

where N is the number of grooves per mm, m is the order of diffraction, and ΔY is the exit slit width. The calculated slit-width limited resolution for the three gratings of the 6m/160° TGM covering an energy range of 8 - 190 eV are given in Table 2. A theoretical resolving power of $E/\Delta E$ = 30,000 at 60 eV with 10 micron vertical exit slit width gives an estimate of how much the performance of the TGM could potentially improve by reducing the aberrations.

3. Monochromator Design and Modifications

The design of the 6m/160° TGM installed on the bending magnet beam line 8-1 at SSRL is similar to several other TGM's, for example at the Synchrotron Radiation Center (SRC) and at the National Synchrotron Light Source (NSLS) [3, 4, 8]. The configuration of TGM 8-1, shown in Fig. 2, has been discussed in detail by Tirsell and Karpenko [9]. The important features to note are the movable exit slit to eliminate the defocus, F_{20}', and the four-way adjustable beam apertures to increase the resolution by masking part of the toroidal grating.

The 6m/160° TGM at SRC provides an example of the typical resolution achieved with the monochromator operated conventionally [8]. With 100 μm slit width, a resolving power $E/\Delta E$ = 1,300 at 47 eV was achieved [8]. Further improvement was precluded by the signal-to-noise ratio in the photoabsorption signal. A somewhat lower resolution of 70 - 90 meV in the photon energy range of 30 - 60 eV was measured at the U4A 6m/160° TGM at NSLS [10]. Note that both TGM's at SRC and NSLS have fixed exit-slit positions, so that the image of the entrance slit is focused by the grating onto the exit slit at only two wavelengths.

To improve the performance of TGM 8-1, the old entrance and exit slits were replaced by high-precision slits based on a flexural design which is used for the Lawrence Berkeley Laboratory Spherical Grating Monochromator on BL 6-1 at SSRL [11]. Both vertical and horizontal apertures are continuously adjustable from a few microns to 2 mm and 4 mm, respectively. The linearity and precision of the slit-width openings were determined with a coordinate measuring machine and also from single-slit diffraction pattern (Fig. 3). A micro-stepping motor (100,000 steps per revolution) controlled by a Mitutoyo linear encoder (Laser Holoscale with a resolution of 10 nm) drives the sine bar which moves the grating. This enabled us to sweep the photon energy in steps of less than one meV.

4. Experimental

The resolution was measured from photoionization spectra of narrow resonance lines in gases with natural linewidths that are much smaller than the value of the monochromator resolution. The gas cell used for the measurements is shown in Fig. 4. The spectra were recorded by measuring the total photoionization current using a two-plate ionization chamber of 25 cm active length filled with 5 - 60 mtorr of gas pressure. One electrode was held at a potential of +20 V. At the second electrode the photoionization current, in the 10^{-10} - 10^{-11} Ampere range, was measured by a Keithley 428 current amplifier. One or two free-standing 1000 Å thick Al windows (Le Bow Corp.), mounted on the seat of the gate valves, separated the ionization cell from the ultrahigh vacuum of the monochromator. When two windows were used, the pressure in the refocusing mirror tank was kept below 5 x 10^{-10} torr by differential pumping between the two windows. If a higher photon flux in the ionization cell was necessary, we used only one window, letting the pressure in the ultrahigh-vacuum part increase to 2 x 10^{-9} torr. A small gas leakage through each window (leak rate ~2x10^{-6} liter torr sec^{-1}) was compensated within one mtorr by leaking gas into the ionization chamber from a gas manifold with a MKS Baratron pressure head and a Granville-Phillips servo-driven valve assembly operated in a closed control loop.

We measured the photonflux with a Si n-on-p photodiode from

United Detector Technology (Model XUV100C), which has a high quantum efficiency in the 25 - 170 eV range, typically 17 electron-hole pairs per photon at 65 eV. The observed photocurrent, in the 10^{-8} - 10^{-9} A range, was measured with a current amplifier. Above 150 eV, the error in the photon flux measurement was less than 4 %, increasing to about 12 % near the Si K-edge.

5. Results

5.1 Photon Flux

Figures 5 and 6 show a scan of the monochromator output over the energy ranges covered by the 823 l/mm and 2400 l/mm gratings, respectively. The decrease in intensity at low photon energies for both gratings is a geometrical effect because more of the beam is missing the optical surface. The decrease in photon flux at high photon energies for the 2400 l/mm grating results from a lower efficiency of the mirrors and grating. The first two mirrors and the gratings of the TGM are coated with Pt. The absorption near the Pt $4f_{7/2}$ and $4f_{5/2}$ edges at 70.9 eV and 74.2 eV, respectively is observed with the 2400 l/mm grating. The same structure is repeated with second order light from the 823 l/mm grating. The absorption feature around 102 eV is due to the Pt 5s edge and absorption by the Si 2p-shell of the SiO_2 overlayer of the Si np-photodiode. This feature can be observed with less intensity with the 823 l/mm grating at energies corresponding to second and third orders of diffraction. The broad absorption feature in the 63 - 70 eV range is due to Pt $5p_{1/2}$ and Ni $3p_{1/2,3/2}$. Nickel is used as coating material for the refocusing mirror.

For the planning of an experiment it is important to know what the available photon flux will be at a certain monochromator resolution. Two of the important parameters determining the monochromator resolution are the horizontal opening of the mask in front of the grating and the vertical opening of the entrance and exit slits (see below). The variation of the photon flux with mask opening and both entrance and exit slit opening shows the expected linear and quadratic dependencies, respectively (see Fig. 7 and 8).

5.2 Energy-resolution Measurement and Data-fitting Procedure

For obtaining the instrumental resolution, the best choice is to measure a photoionization spectrum from a gas sample with a natural linewidth smaller than or comparable with the instrumental contribution. We studied the inert gases He and Ne with suitable absorption edges at energies covered by the 823 l/mm grating. However, for the systematic study of the monochromator resolution on various parameters, the He photoionization $1s^2 \rightarrow (2s4p+2p4s)$ Rydberg state with an experimental linewidth of 5 ± 1 meV [12] was measured. A typical spectrum (double-excitation Rydberg state near 64.5 eV [12]) with pronounced Fano profile [13] is shown in Figure 9a (dotted points).

The value of the monochromator resolution was determined in two ways: One approach was to deconvolute the experimental spectra by dividing its Fourier transform by a Fourier transform of a Fano function. After taking the inverse Fourier transform, the monochromator function would emerge. This instrumental function was then fitted with a symmetrical Gaussian function assuming that resolution of the TGM is equal to the FWHM of the Gaussian function. The second approach was based on a least-square fit of the experimental spectra with a numerical convolution of a Shore function [14] with a Gaussian function. The first approach has the advantage that it gives the pure instrumental function, and non-Gaussian contributions to the instrumental function, can be detected (see Fig. 9b). Its disadvantage is the great sensitivity of the Fourier transformation to noise in the spectra. The second approach gave in some cases better fits of the experimental spectra. Nevertheless, the derived values for the monochromator resolution agree within 1 meV for both fitting procedures.

5.3 Resolution Versus Exit Slit Position

One of the largest terms contributing to the monochromator linewidth is the defocus, F_{20}. This term can be eliminated by moving the exit slit to the vertical focus position for a given wavelength. Figure 10

shows the effect of the exit-slit position on the resolution of the monochromator determined at photon energies of 31.8 eV (He {sp,23+} state in second order), 47 eV (Ne $\{2s^{-1}\ 4p\}$ state) and 64.5 eV (He {sp,24+} state) while the other terms were kept constant. The measurements at 31.8 eV were performed with old entrance and exit slits and the data for 47.0 eV and 64.5 eV were obtained after the installation of the high-precision slits. It is obvious from the figure that the resolution depends strongly on the exit-slit distance. This shows the importance of a movable exit slit for achieving a high resolution over the available energy range.

Fig. 10 shows a comparison of the experimental exit-slit distances with calculations assuming $F_{20}' = 0$. The calculation of the theoretical exit-slit distance was performed by B. Tonzet (Instruments SA-Division Jobin-Yvon) for our holographically produced, aberration-reduced toroidal grating [15]. The experimental exit-slit distances at 31.8 eV, 47.0 eV, and 64.5 eV are larger than the theoretical values by 3.2 cm, 8.0 cm, and 7.5 cm, respectively. The small difference of 3.2 cm for the measurement with the old slits shows that the design parameters of the TGM do not agree completely with the anticipated values. The difference between the data obtained before and after the installation of the high-precision slits is due to a design related change of BL 8-1. The change in the slit positions inside the slit housing has not been included in the calculations. Therefore for TGM 8-1, an offset of 7.5 - 8.0 cm should be added to the theoretical exit-slit distance to eliminate the defocus term. All experimental data shown in this paper were obtained with the exit slit at the focus position.

5.4 Resolution Versus Slit Openings

Figure 11 shows the measured monochromator linewidth as a function of the vertical entrance and exit-slit openings, which were changed simultaneously. The horizontal apertures were kept at 2 mm. The measurements were carried out at a photon energy of 64.5 eV and with 32% mask opening of the grating. The data move away from a straight line around a 50 micron slit opening. In the range between 50 and 100 microns, and presumably for larger slit openings, the data approach the slit-width limited performance with a dispersion of 0.24-0.23 eV/mm, as

expected by theory (see Table 2). The ultimate resolution, at lower slit openings, is limited by the aberrations. The data also indicate a maximum resolving power of 13,000 for 10 μm vertical slit settings and 32% horizontal mask opening of the grating. Higher resolution is expected if the grating is also masked in the vertical plane.

Figure 12 shows the effect of the horizontal exit-slit opening on the resolution of the monochromator. There is no significant change in resolution for exit-slit widths in the range of 1-3 mm. However, at lower slit widths the resolution improves.

5.5 Resolution Versus Masking

The effect of masking a part of the grating to reduce aberrations and thus improve the resolving power of the monochromator is shown in Fig. 13. The data were obtained for vertical entrance and exit-slit openings of 10 μm and 20 μm. The horizontal entrance/exit aperture was kept at 3 mm/2 mm. Because without masking the monochromator resolution is the same for 10 μm and 20 μm slit width, the resolution is not slit-width limited but determined by the aberrations of the grating. As can be seen from Fig. 13, the aberration decreases with increased masking of the grating. The intercepts of linear fits through the two sets of data points taken at vertical slit openings of 20 micron and 10 micron provide the ultimate achievable monochromator linewidths of 6.2 meV and 3.7 meV, respectively, at horizontal mask openings approaching zero. The calculated slit-width limited resolution at 20 μm and 10 μm are 4.5 meV and 2.2 meV, respectively. This indicates that for achieving the slit-width limited resolution one should try masking the grating vertically, as well as horizontally, to reduce ray aberrations due to the w^2 aberration and fabrication errors. In addition, higher precision in the alignment of the entrance and exit slits with each other may be required to achieve the ultimate goal.

6. Conclusion

We have shown that it is possible to achieve ultrahigh resolution, at the expense of the flux, in the soft x-ray energy range from a

conventional, moderate-resolution Toroidal Grating Monochromator with a movable exit slit. An ultimate resolving power of 13,000 was obtained by improving the accuracy of the entrance and exit slits as well as the driving mechanism, and by horizontally masking about half of the grating. To achieve the slit-width limited resolution, it will also be desirable to mask a vertical portion of the grating as well as to improve the precision in the alignment of the slits.

Acknowledgment:

We thank P. Pianetta and M. Weber for their help in the development of the slits and G. Husek for fabricating the slits and mounting of the encoder. We appreciate the efforts of M. Rowen and the SSRL vacuum group. We acknowledge Bob Fancy of Acton Research Corporation for useful discussions about the design of the slits and the monochromator. We thank W.R. McKinney for useful discussions. This work was supported by the Director, Office of Energy Research, Office of Basic Energy Sciences, Chemical Sciences Division of the U. S. Department of Energy, LBL under Contract No. DE-AC03-76SF00098, LLNL under contract number W-7405-ENG-48. G. K. was supported by the Bundesminister für Forschung und Technologie, Project No. 05-5KEAXI3/TP03. T. R. thanks the Alexander von Humboldt Foundation for support through a Feodor Lynen Fellowship, and Penn State University for additional support.

References

1. M. R. Howells, Nucl. Instr. and Meth. **172** (1980)123.

2. W. R. McKinney and M. R. Howells, Nucl. Instr. and Meth. **172** (1980)149.

3. F. J. Himpsel, Y. Jugnet, D. E. Eastman, J. J. Donelon, D. Grimm, G. Landgren, A. Marx, J. F. Morar, C. Oden, R. A. Pollak, and J. Schneir, Nucl. Instr. and Meth. **222** (1984)107.

4. P. Thiry, P. A. Bennett, S. D. Kevan, W. A. Royer, E. E. Chaban, J. E. Rowe, and N. V. Smith, Nucl. Instr. and Meth. **222** (1984)85.

5. P. Thiry and N. V. Smith, Nucl. Instr. and Meth. **222** (1984)91.

6. C. T. Chen, E. W. Plummer, and M. R. Howells, Nucl. Instr. and Meth. **222** (1984)103.

7. H. Noda, T. Namioka, and M. Seya, J. Opt.Soc. **64** (1974)1031.

8. J. L. Rose, D. C. Mancini, J. T. Welnak, and R. K. Cole, Nucl. Instr. and Meth. **A291** (1990)192.

9. K. G Tirsell and V. P. Karpenko, Nucl. Instr. and Meth. **A291** (1990)511.

10. G. K. Wertheim, J. E. Rowe, and D. N. E. Buchanan, NSLS Annual Report (1988)91.

11. P. A. Heimann, F. Senf, W. R. McKinney, M. R. Howells, R. D. van Zee, L. J. Medhurst, T. Lauritzen, J. Chin, J. Meneghetti, W. Gath, H. Hogrefe, and D. A. Shirley, Phys. Scr. **T31** (1990)127.

12. M. Domke, C. Xue, A. Puschmann, T. Mandel, E. Hudson, D. A. Shirley, G. Kaindl, C. H. Greene, H. R. Sadeghpour, and H. Petersen,

Phys. Rev. Lett. **66** (1991)1306.

13. U. Fano, Phys. Rev. **124** (1961)1866 .

14. B. W. Shore, Phys. Rev. **171** (1968)43.

15. B. Tonzet, private communication

Figure Captions

1. Coordinate system used to discuss the optical system (from Ref. 7).

2. Schematic drawing of the Toroidal Grating Monochromator on BL 8-1 (from Ref. 9).

3. Measured slit width as a function of micrometer setting.

4. Schematic drawing of a photoionization gas cell with differential pumping.

5. The monochromator output from the 823 l/mm grating detected with a Si photodiode and normalized to 100 mA ring current. The horizontal/vertical opening of the entrance and exit slits were 3 mm/200 μm and 1.5 mm/200 μm, respectively.

6. The monochromator output from the 2400 l/mm grating detected with a Si photodiode and normalized to 100 mA ring current. The horizontal/vertical opening of the entrance and exit slits were 3 mm/300 μm and 1.5 mm/150 μm, respectively.

7. The measured photon flux at 64.9 eV plotted against horizontal mask opening for three different vertical entrance and exit-slit settings. The horizontal entrance and exit slits were fixed at 1.7 mm and 2.0 mm, respectively. The solid line is a linear least-square fit to the data.

8. The measured photon flux at 64.9 eV plotted against vertical entrance and exit-slit openings for three different horizontal mask openings. The solid line is a quadratic least-square fit to the data.

9. a) Photoionization spectrum from He gas showing the autoionizing double-excitation state of He $(sp,24+)^1P^0$. The spectrum was obtained with entrance and exit slits of 10 μm and 32% mask opening of the grating. The solid curve is a fit with G_{Fano} = 5.0 meV and $G_{Gaussian}$ = 5.0 meV.

b) The monochromator function after deconvolution (dots) and fits with a symmetrical Gaussian function (solid line) and an asymmetrical Gaussian function (dashed line). The photoionization spectrum was measured with 30 μm vertical entrance and exit-slit opening.

10. The measured monochromator linewidth (FWHM) as a function of the exit-slit distance. Entrance- and exit-slit vertical openings were kept at 20 μm with 48% mask opening of the grating. The resolution was determined by fitting a He double-excitation peak at 64.5 eV and at 31.8 eV (with second order light) and a Ne state at 47 eV. The 47 eV curve is incomplete, with the data extending barely through the minimum. The vertical lines at the bottom of the figure indicate the theoretical exit-slit distances for $F_{20}^{'} = 0$ [15].

11. The measured monochromator linewidth (FWHM) at 64.5 eV plotted versus equal opening of vertical slits. The horizontal entrance/exit apertures were kept at 3 mm/2 mm. The horizontal mask opening was 32 %.

12. The measured monochromator linewidth (FWHM) at 64.5 eV plotted versus horizontal exit-slit opening. The vertical entrance/exit slits were kept at 10 μm /10 μm. The horizontal mask opening was 48 %.

13. The measured monochromator linewidth (FWHM) at 64.5 eV plotted versus horizontal mask opening for vertical entrance and exit-slit openings of 10 μm and 20 μm. The horizontal entrance/exit aperture was kept at 3 mm/2 mm. The solid line is a linear least-square fit to the data.

Table 1. Values for M_{ij} and H_{ij} in Eq. (3).

$$M_{ij} = E_{ij}(\alpha, \mathrm{r}) + E_{ij}(\beta, \mathrm{r}')$$
$$H_{ij} = E_{ij}(\gamma, \mathrm{r_C}) - E_{ij}(\delta, \mathrm{r_D})$$

$$E_{20}(\alpha, \mathrm{r}) = \frac{1}{2}\frac{\cos^2\alpha}{\mathrm{r}} - \mathrm{a}_{20}\cos\alpha$$
$$E_{02}(\alpha, \mathrm{r}) = \frac{1}{2\mathrm{r}} - \mathrm{a}_{02}\cos\alpha$$
$$E_{12}(\alpha, \mathrm{r}) = \frac{\sin\alpha}{2\mathrm{r}^2} - \mathrm{a}_{02}\frac{\sin\alpha\cos\alpha}{\mathrm{r}} - \mathrm{a}_{12}\cos\alpha$$

Table 2. Ideal peformance for the R=19.224 m grating and a vertical exit-slit width of Y=10μm.

Grating	Photon energy (eV)	Reciprocal linear dispersion (eV/mm)	Slit-width limited resolving power E/ΔE (FWHM)
2400 l/mm	200	0.746	26,700
	150	0.447	33,600
	100	0.222	45,000
	75	0.139	54,000
823 l/mm	80	0.338	23,700
	60	0.201	29,900
	40	0.099	40,400
	20	0.032	62,500
288 l/mm	25	0.096	26,000
	20	0.065	30,800
	15	0.039	38,500
	10	0.020	50,000

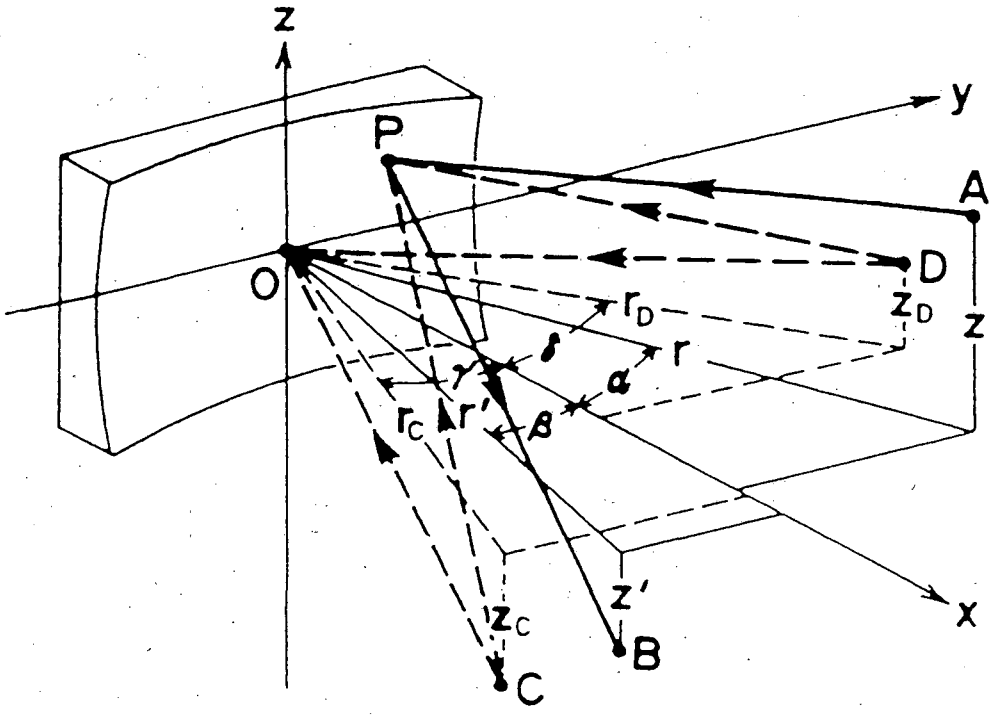

XBL 932-196

Figure 1

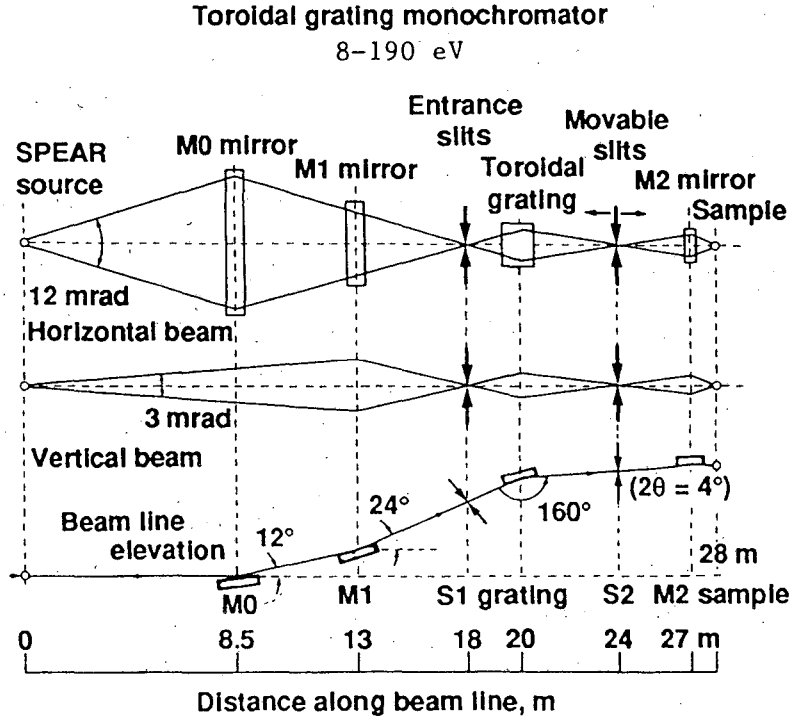
Toroidal grating monochromator
8-190 eV
SPEAR source
M0 mirror
M1 mirror
Entrance slits
Toroidal grating
Movable slits
M2 mirror
Sample
12 mrad
Horizontal beam
3 mrad
Vertical beam
Beam line elevation
12°
24°
160°
(2θ = 4°)
28 m
M0
M1
S1 grating
S2
M2 sample
0
8.5
13
18
20
24
27 m
Distance along beam line, m
XBL 931-20

Figure 2

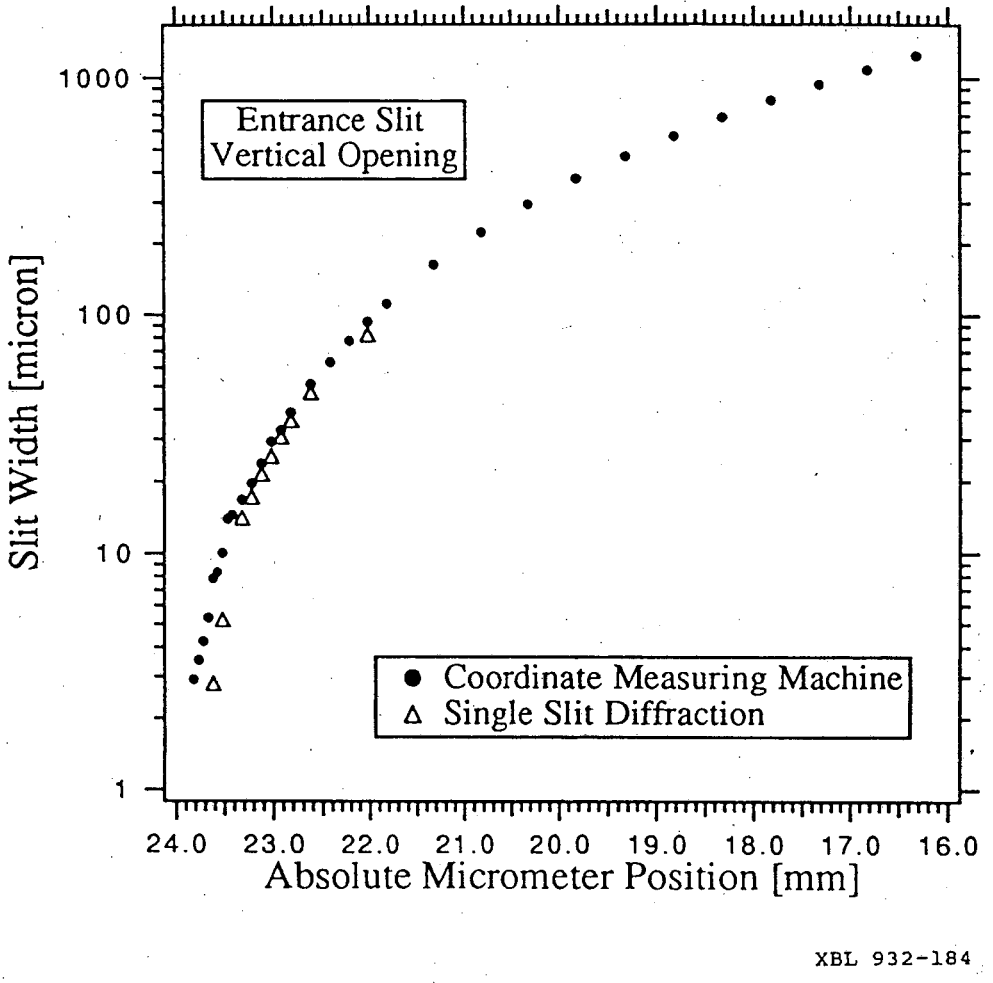
Entrance Slit
Vertical Opening
Slit Width [micron]
1000
100
10
1
Coordinate Measuring Machine
Single Slit Diffraction
24.0
23.0
22.0
21.0
20.0
19.0
18.0
17.0
16.0
Absolute Micrometer Position [mm]
XBL 932-184

Figure 3

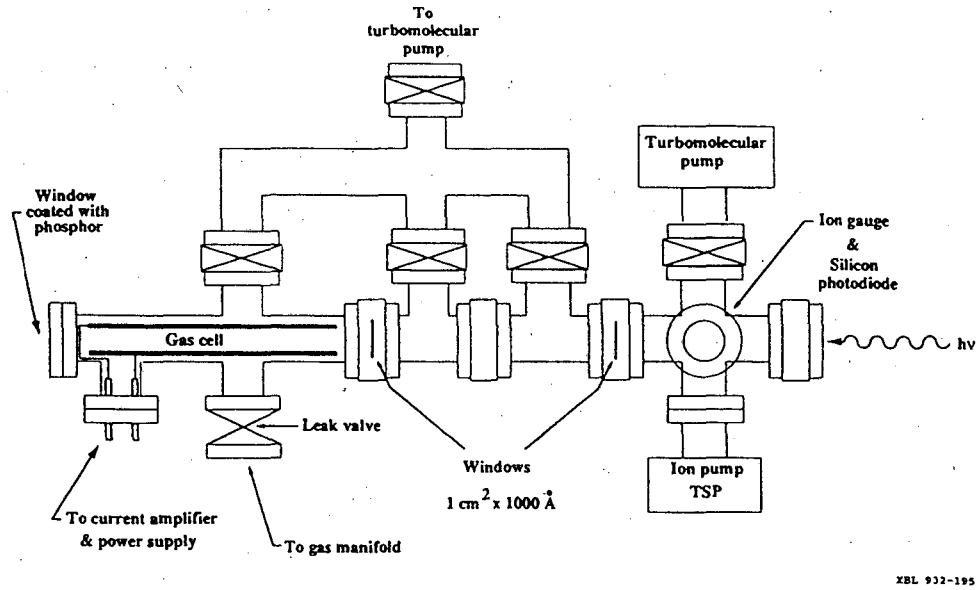
To
turbomolecular
pump
Turbomolecular
pump
Window
coated with
phosphor
Ion gauge
&
Silicon
photodiode
Gas cell
hv
Leak valve
Windows
1 cm^2 x 1000 Å
Ion pump
TSP
To current amplifier
& power supply
To gas manifold
XBL 932-195

Figure 4

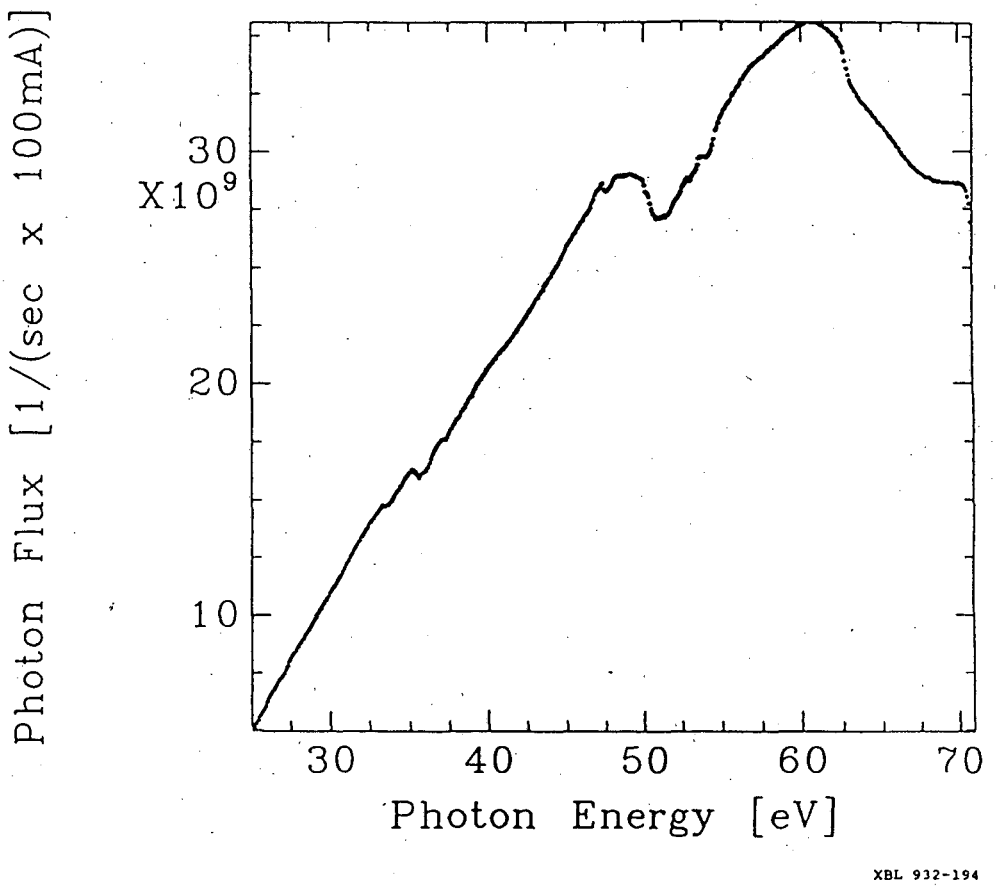
Photon Flux [1/(sec x 100mA)]
30
X10^9
20
10
30
40
50
60
70
Photon Energy [eV]
XBL 932-194

Figure 5

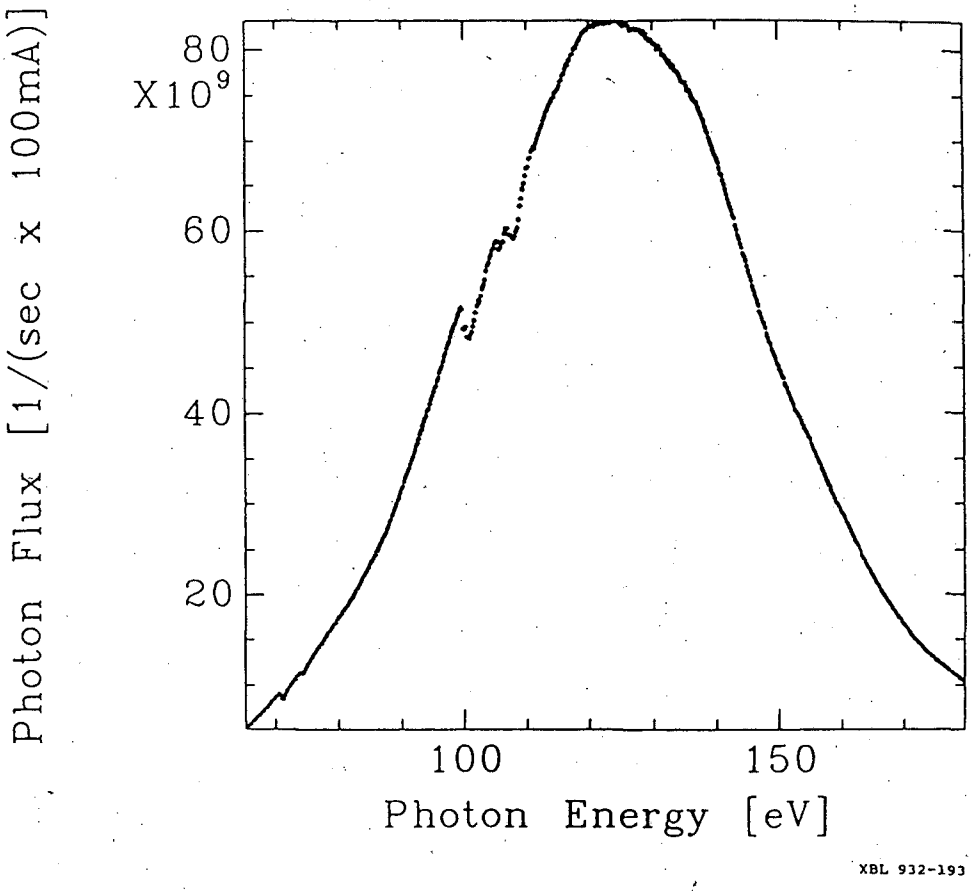
Photon Flux [1/(sec x 100mA)]
80
X10^9
60
40
20
100
150
Photon Energy [eV]
XBL 932-193

Figure 6

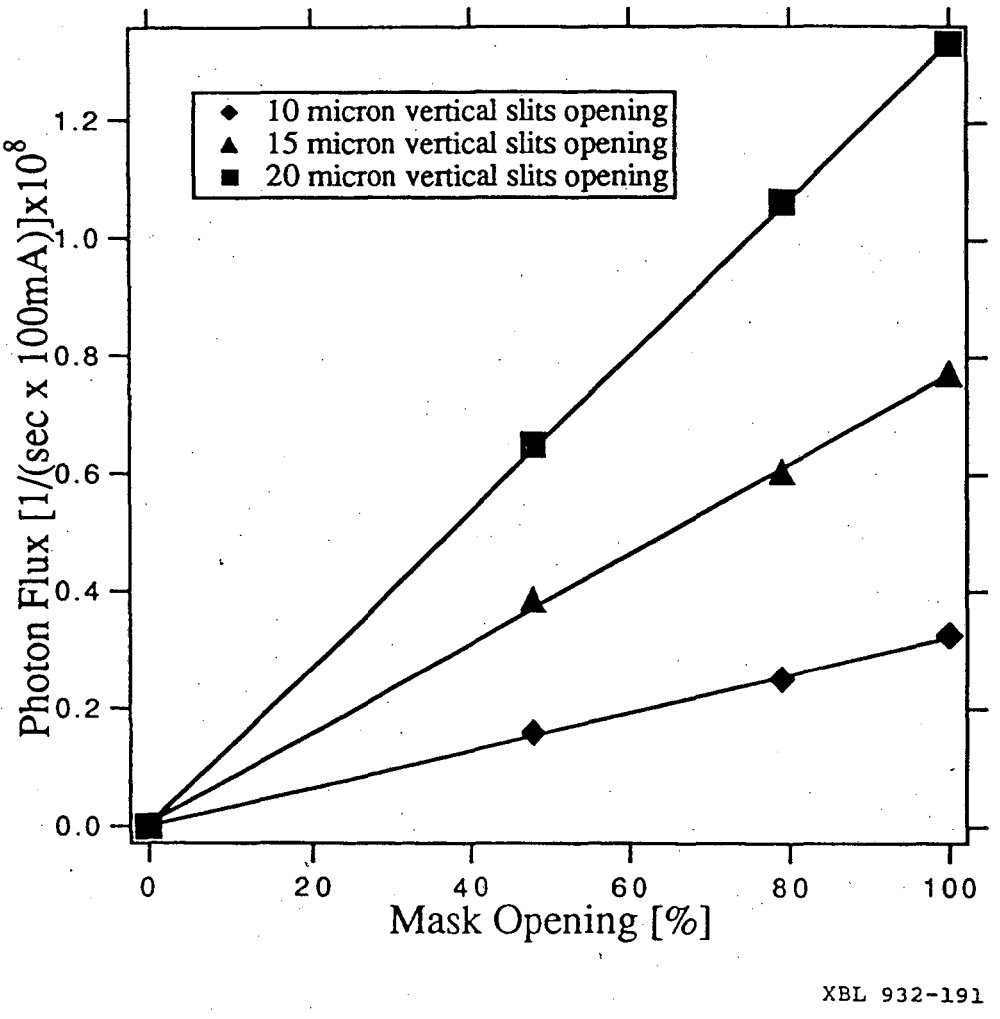
10 micron vertical slits opening
15 micron vertical slits opening
20 micron vertical slits opening
Photon Flux [1/(sec x 100mA)]x10^8
0.0
0.2
0.4
0.6
0.8
1.0
1.2
0
20
40
60
80
100
Mask Opening [%]
XBL 932-191

Figure 7

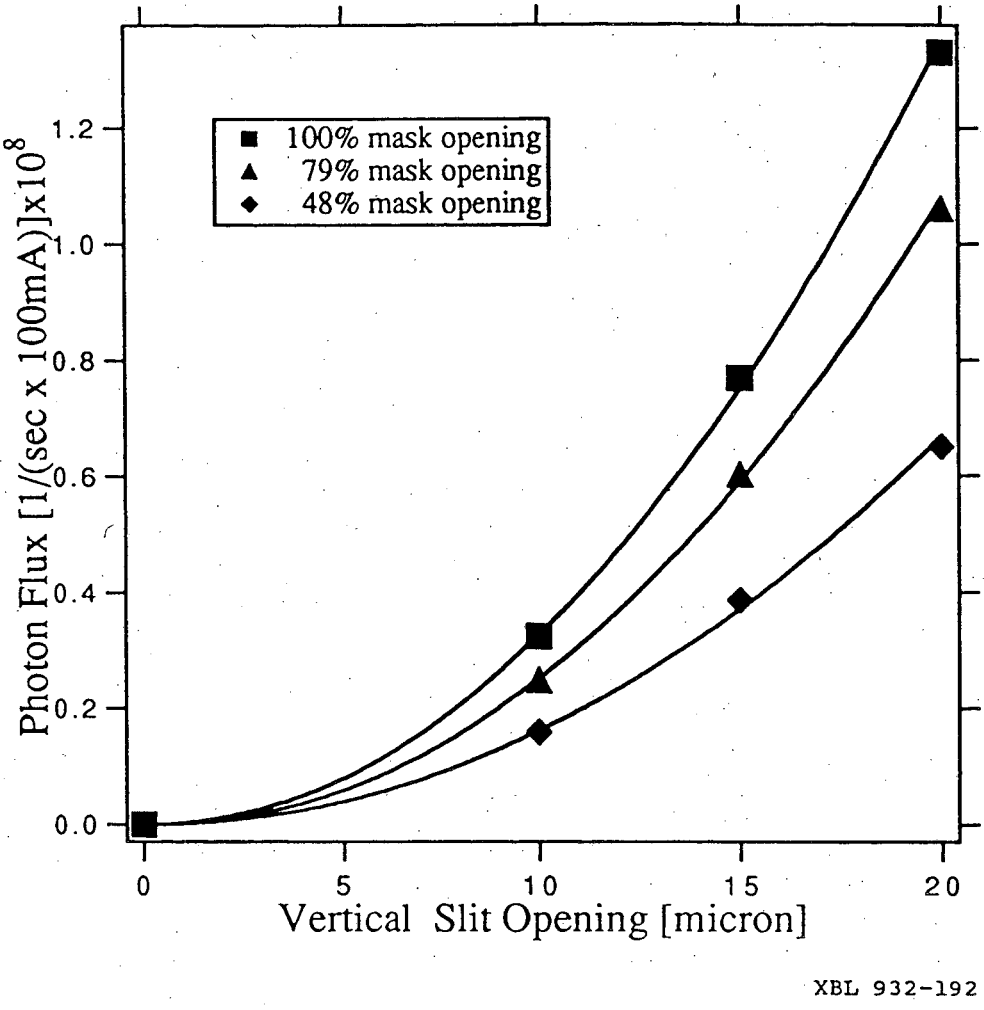
100% mask opening
79% mask opening
48% mask opening
Photon Flux [1/(sec x 100mA)]x10^8
1.2
1.0
0.8
0.6
0.4
0.2
0.0
0
5
10
15
20
Vertical Slit Opening [micron]
XBL 932-192

Figure 8

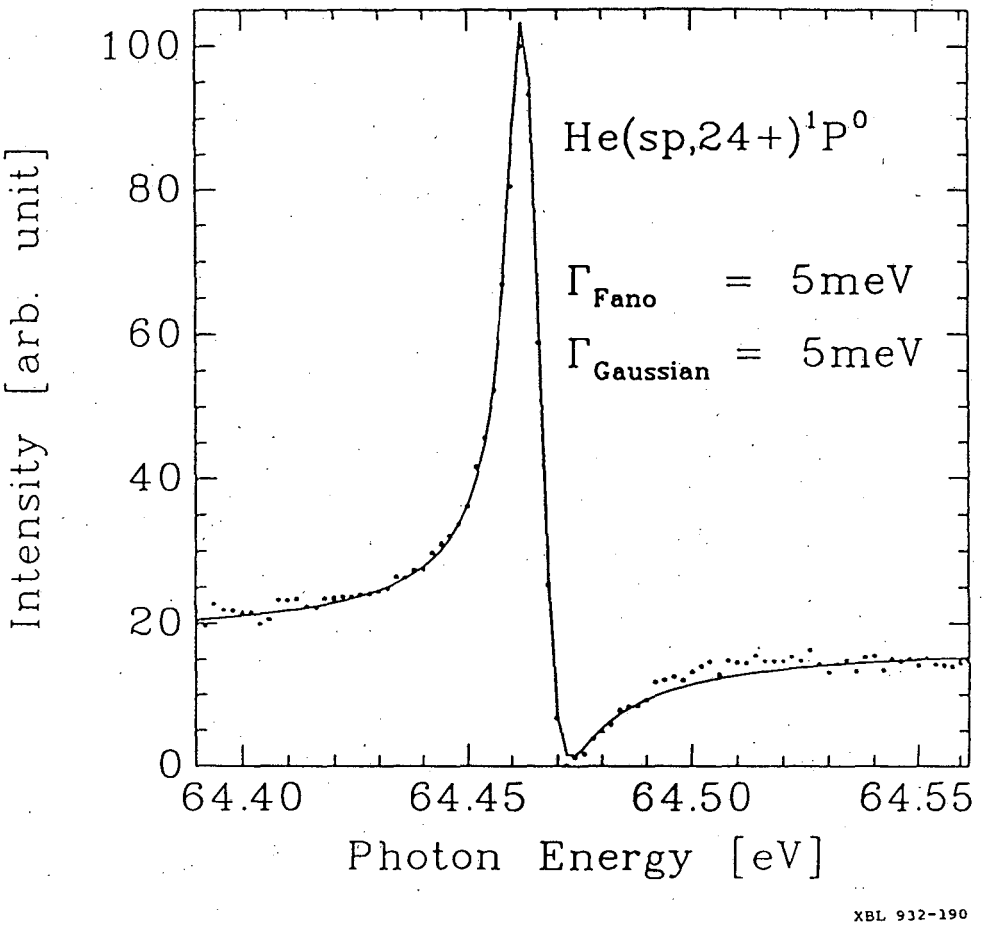
100
80
60
40
20
0
Intensity [arb. unit]
64.40
64.45
64.50
64.55
Photon Energy [eV]
He(sp,24+)$^1P^0$
Γ_{Fano} = 5meV
$\Gamma_{Gaussian}$ = 5meV
XBL 932-190

Figure 9 a)

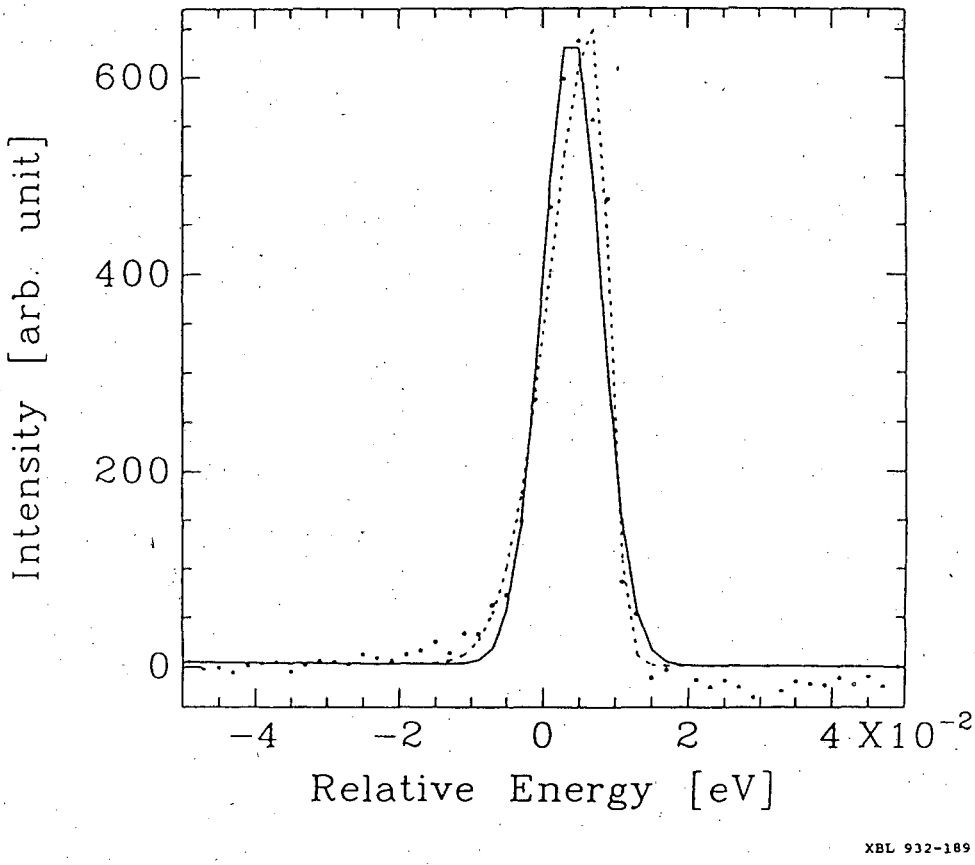
600
400
200
0
Intensity [arb. unit]
−4
−2
0
2
4 X10^{-2}
Relative Energy [eV]
XBL 932-189

Figure 9 b)

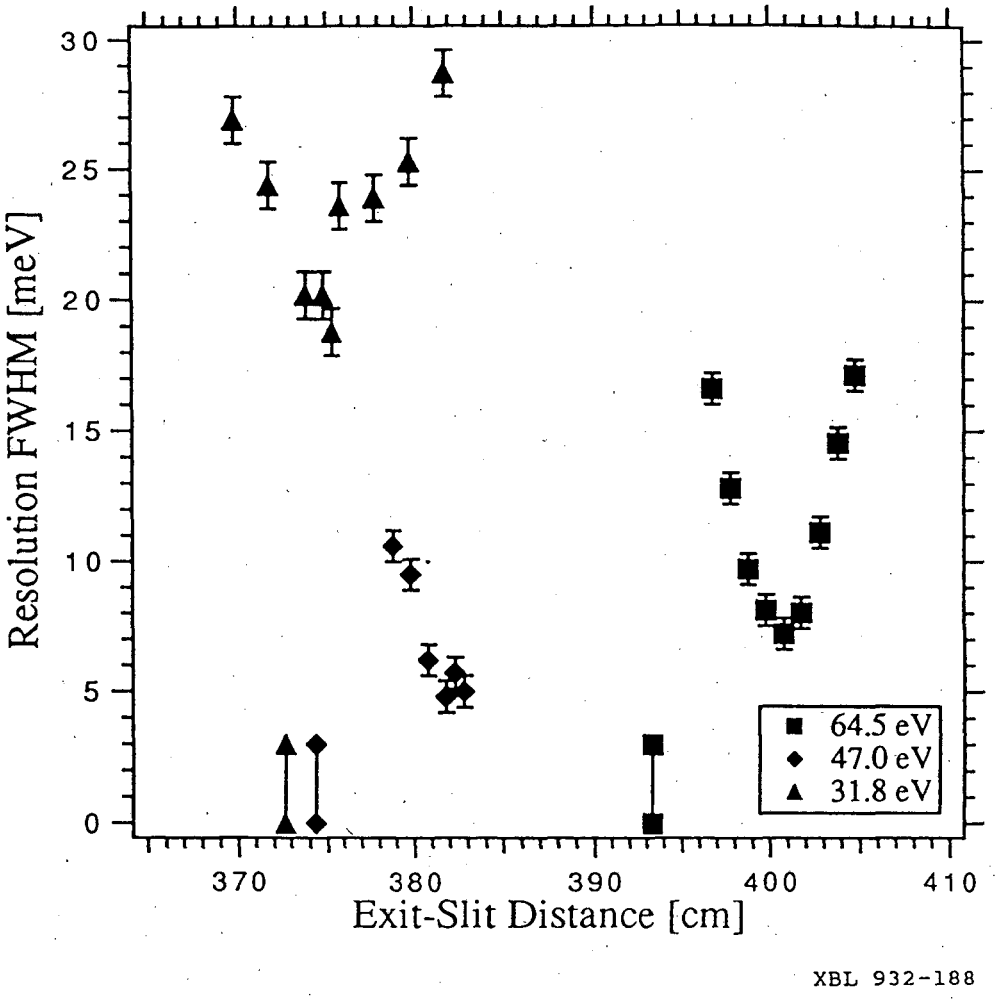
Resolution FWHM [meV]
30
25
20
15
10
5
0
370
380
390
400
410
Exit-Slit Distance [cm]
64.5 eV
47.0 eV
31.8 eV
XBL 932-188

Figure 10

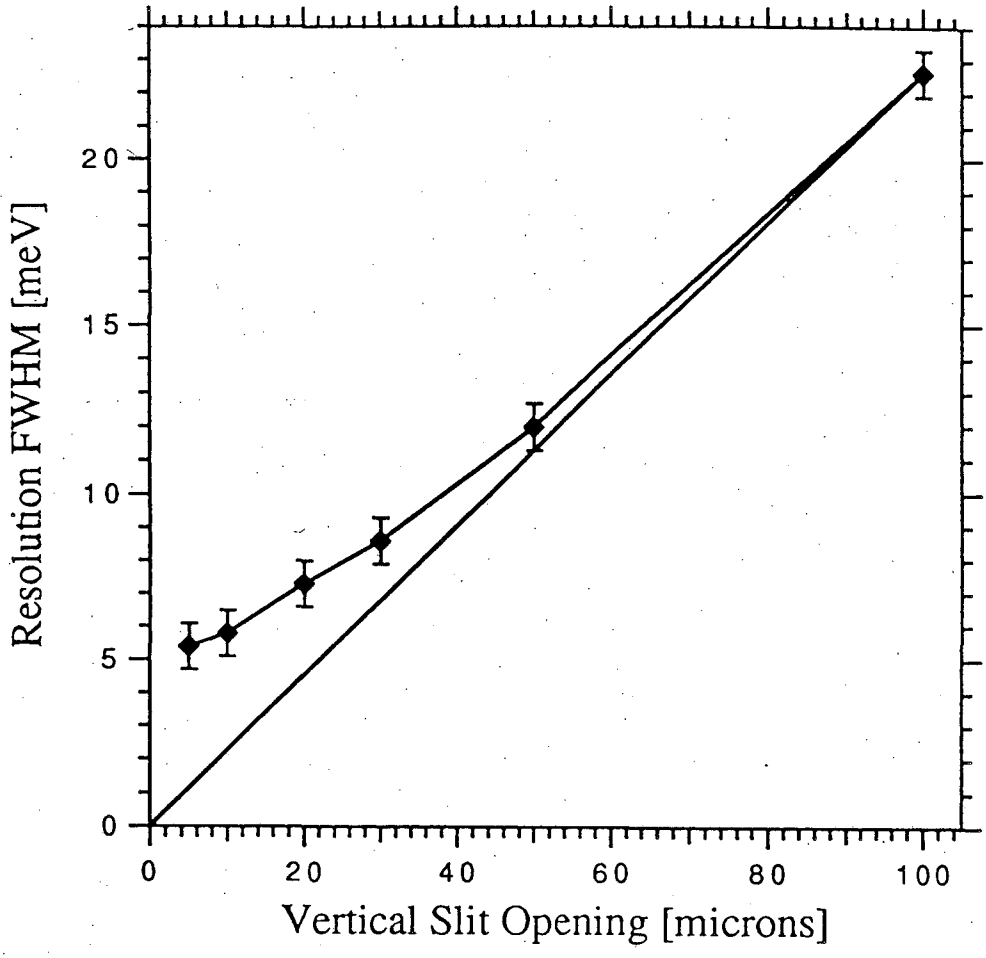
Resolution FWHM [meV]
0
5
10
15
20
0
20
40
60
80
100
Vertical Slit Opening [microns]
XBL 932-187

Figure 11

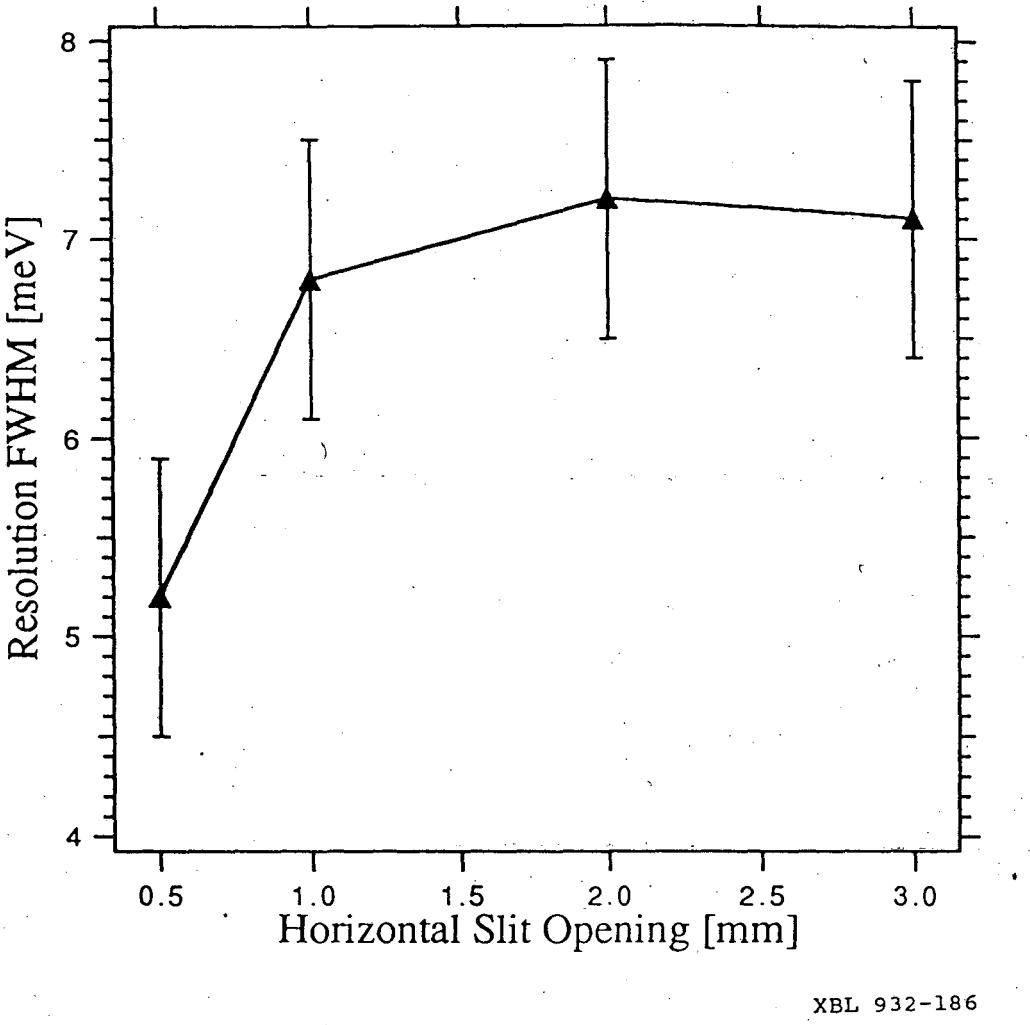
Resolution FWHM [meV]
8
7
6
5
4
0.5
1.0
1.5
2.0
2.5
3.0
Horizontal Slit Opening [mm]
XBL 932-186

Figure 12

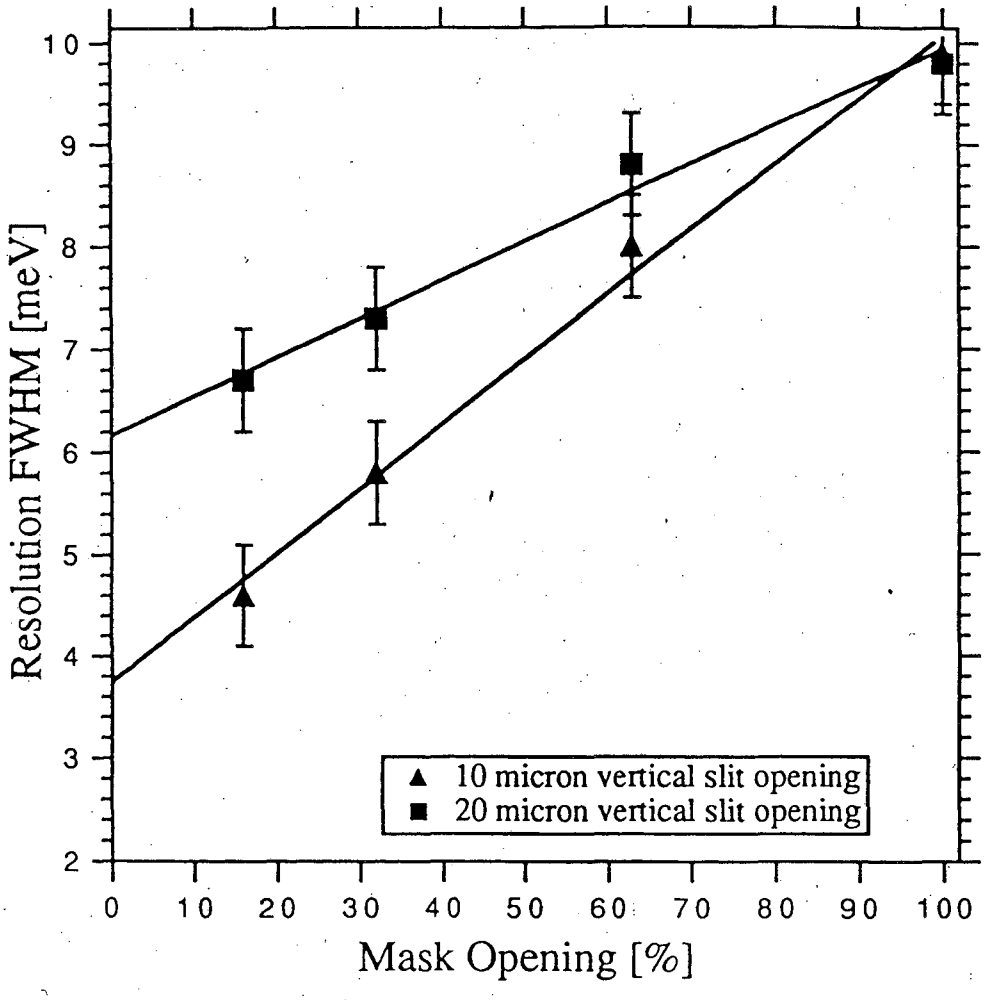
Resolution FWHM [meV]
Mask Opening [%]
10 micron vertical slit opening
20 micron vertical slit opening
XBL 932-185

Figure 13

LAWRENCE BERKELEY LABORATORY
UNIVERSITY OF CALIFORNIA
TECHNICAL INFORMATION DEPARTMENT
BERKELEY, CALIFORNIA 94720